HIGH ENERGY COSMIC RAY AND ACCELERATOR CROSS SECTIONS RECONCILED

MARTIN BLOCK

Department of Physics and Astronomy, Northwestern University
Evanston, IL 60208, USA

E-mail: mblock@northwestern.edu

ABSTRACT

The energy range of cosmic ray experiments covers not only the energy of the Large Hadron Collider (LHC), but extends beyond it. Extracting proton–proton cross sections from cosmic ray observations is far from straightforward. Cosmic ray experiments map the atmospheric depth at which cosmic ray initiated showers develop, by measuring the shower attenuation length (Λ_m), which is not only sensitive to the interaction length of the protons in the atmosphere ($\lambda_{p-\rm air}$), with $\Lambda_m = k\lambda_{p-\rm air} = k\frac{14.5m_p}{\sigma^{\rm inel}_{p-\rm air}}$, but also depends critically on the proton inelasticity and the properties of the pion interactions, which determines the rate at which the energy of the primary proton is dissipated into electromagnetic shower energy observed in the experiment. This is taken into account by the parameter k. The departure of k from unity depends on the inclusive particle production cross section in nucleon and meson interactions on the light nuclear target of the atmosphere and its energy dependence. We *simultaneously* fit a QCD-inspired parameterization of all accelerator data on forward proton-proton and antiproton-proton scattering amplitudes, *together* with cosmic ray data (using Glauber theory), to predict proton–air and proton-proton cross sections at energies near $\sqrt{s} \approx 30$ TeV. We also show that, using the additive quark model, along with vector dominance, that we successfully predict γp and $\gamma\gamma$ cross sections. We find that the p-air cosmic ray measurements strongly constrain the inclusive particle production cross section, as well as reducing the errors on the fit parameters—in turn, markedly reducing the errors in the high energy proton-proton and proton-air cross section predictions. An accurate measurement of $\sigma_{\rm tot}$ at the LHC would, in turn, again greatly reduce the errors for cosmic ray predictions. A high energy parameterization of $\sigma^{\rm inel}_{p-\rm air}$, useful for calculating neutrino fluxes, is given. We also give predictions for the LHC.

1. Introduction

This communication is divided into 3 parts

- Part 1: fitting total cross sections, ρ values (ρ is the ratio of the real to the imaginary portion of the forward scattering amplitude) and B, the nuclear slope parameter ($B(s) = \frac{d}{dt}[\ln\frac{d\sigma}{dt}(s,t)]_{t=0}$) to accelerator data—$pp$ and $\bar{p}p$—using a QCD-inspired eikonal model.

- Part 2: predicting γp and $\gamma\gamma$ cross sections from the nucleon-nucleon fit, using a naive quark model and vector dominance, using the eikonal model.

- Part 3: making a global fit using *both* cosmic ray and accelerator data *simultaneously*, to predict $\sigma_{p-\mathrm{air}}^{\mathrm{inel}}$ and σ_{pp} at ultra-high ($E_{\mathrm{lab}} > 10^{18}$ ev) energies.

2. Fitting Accelerator Data using a QCD-Inspired Eikonal Model

We use an eikonal model to make calculations of cross sections, nucleon slope parameters B and ρ values in $\bar{p}p$ and pp collisions, work done by Block, Gregores, Halzen and Pancheri[1].

We define our (complex) eikonal $\chi(b,s)$ so that $a(b,s)$, the (complex) scattering amplitude in impact parameter space b, is given by

$$a(b,s) = \frac{i}{2}\left(1 - e^{i\chi(b,s)}\right) = \frac{i}{2}\left(1 - e^{-\chi_{\mathrm{I}}(b,s)+i\chi_{\mathrm{R}}(b,s)}\right). \tag{1}$$

Using the optical theorem, the total cross section $\sigma_{\mathrm{tot}}(s)$ is given by

$$\sigma_{\mathrm{tot}}(s) = 2\int \left[1 - e^{-\chi_{\mathrm{I}}(b,s)}\cos(\chi_{\mathrm{R}}(b,s))\right]\, d^2\vec{b}, \tag{2}$$

the elastic scattering cross section $\sigma_{\mathrm{el}}(s)$ is given by

$$\sigma_{\mathrm{elastic}}(s) \quad = \quad \int \left|1 - e^{-\chi_{\mathrm{I}}(b,s)+i\chi_{\mathrm{R}}(b,s)}\right|^2\, d^2\vec{b}. \tag{3}$$

The ratio of the real to the imaginary portion of the forward nuclear scattering amplitude, ρ, is given by

$$\rho(s) \quad = \quad \frac{\mathrm{Re}\left\{i(\int 1 - e^{-\chi_{\mathrm{I}}(b,s)+i\chi_{\mathrm{R}}(b,s)})\, d^2\vec{b}\right\}}{\mathrm{Im}\left\{i(\int(1 - e^{-\chi_{\mathrm{I}}(b,s)+i\chi_{\mathrm{R}}(b,s)})\, d^2\vec{b}\right\}} \tag{4}$$

and the nuclear slope parameter B is given by

$$B = \frac{1}{2}\frac{\int\left(1 - e^{-\chi_{\mathrm{I}}(b,s)+i\chi_{\mathrm{R}}(b,s)}\right)\, b^2\ d^2\vec{b}}{\int\left(1 - e^{-\chi_{\mathrm{I}}(b,s)+i\chi_{\mathrm{R}}(b,s)}\right)\ d^2\vec{b}}\ . \tag{5}$$

Block *et al.*[1] have used an even QCD-Inspired eikonal χ_{even} given by the sum of three contributions, glue-glue, quark-glue and quark-quark, which are individually factorizable into a product of a cross section $\sigma(s)$ times an impact parameter space distribution function $W(b\,;\mu)$, *i.e.,*:

$$\begin{aligned}\chi^{\mathrm{even}}(s,b) &= \chi_{\mathrm{gg}}(s,b) + \chi_{\mathrm{qg}}(s,b) + \chi_{\mathrm{qq}}(s,b) \\ &= i\left[\sigma_{\mathrm{gg}}(s)W(b\,;\mu_{\mathrm{gg}}) + \sigma_{\mathrm{qg}}(s)W(b\,;\mu_{\mathrm{qg}}) + \sigma_{\mathrm{qq}}(s)W(b\,;\mu_{\mathrm{qq}})\right],\end{aligned} \tag{6}$$

where we have set $\mu_{\mathrm{qg}} = \sqrt{\mu_{\mathrm{qq}}\mu_{\mathrm{gg}}}$ and where the impact parameter space distribution function

$$W(b\,;\mu) = \frac{\mu^2}{96\pi}(\mu b)^3 K_3(\mu b) \tag{7}$$

is normalized so that $\int W(b\,;\mu)d^2\vec{b} = 1$. Hence, the σ's in eq. (6) have the dimensions of a cross section. The factor i is inserted in eq. (6) since the high energy eikonal is largely imaginary (the ρ value for nucleon-nucleon scattering is rather small). The total even contribution is not yet analytic. For large s, the even amplitude in eq. (6) is made analytic by the substitution $s \rightarrow se^{-i\pi/2}$ (see the table on p. 580 of reference [2]), along with reference [3]). The quark contribution $\chi_{\rm qq}(s,b)$ accounts for the constant cross section and a Regge descending component ($\propto 1/\sqrt{s}$), whereas the mixed quark-gluon term $\chi_{\rm qg}(s,b)$ simulates diffraction ($\propto \log s$). The glue-glue term $\chi_{\rm gg}(s,b)$, which eventually rises as a power law s^ϵ, accounts for the rising cross section and dominates at the highest energies. In eq. (6), the inverse sizes (in impact parameter space) $\mu_{\rm qq}$ and $\mu_{\rm gg}$ are to be fit by experiment, whereas the quark-gluon inverse size is taken as $\mu_{\rm qg} = \sqrt{\mu_{\rm qq}\mu_{\rm gg}}$.

The high energy analytic *odd* amplitude (for its structure in s, see eq. (5.5b) of reference [2]), with $\alpha = 0.5$) that fits the data is given by

$$\chi_{\rm I}^{\rm odd}(b,s) \quad = \quad -\sigma_{\rm odd}\, W(b;\mu_{\rm odd}), \tag{8}$$

with $\sigma_{\rm odd} \propto 1/\sqrt{s}$, and with $W(b,\mu_{\rm odd}) = \frac{\mu_{\rm odd}^2}{96\pi}(\mu_{\rm odd}b)^3\, K_3(\mu_{\rm odd}b)$ normalized so that $\int W(b\,;\mu_{\rm odd})d^2\vec{b} = 1$.

Finally,

$$\chi_{pp}^{\bar{p}p} = \chi_{\rm even} \pm \chi_{\rm odd}. \tag{9}$$

The eikonal of eq. (6) is a QCD-inspired parameterization of the forward proton–proton and proton–antiproton scattering amplitudes which is analytic, unitary, satisfies crossing symmetry, the Froissart Bound (asymptotically approaching a black disk) and, using a χ^2 procedure, fits all accelerator data of $\sigma_{\rm tot}$ (including the new E-811 Tevatron cross section[4]), nuclear slope parameter B and ρ, the ratio of the real-to-imaginary part of the forward scattering amplitude for both pp and $\bar{p}p$ collisions (for details, see reference [1]). We fit all the highest energy cross section data (E710[5], CDF [6] and the new E-811 Tevatron value[4]), which anchor the upper end of our cross section curves. The results of the fit are shown in Fig. 1. Data for ρ values and B are confronted with our model in Figs. 2 and 3.

It can be seen from those figures that we obtain a satisfactory description of all 3 quantities, for both $\bar{p}p$ and pp scattering. The χ^2 of the fit is reasonably good (considering the large spread in some of the experimental data, as well as the discrepancies in the highest energy cross sections), giving a $\chi^2/d.f. = 1.66$, for 75 degrees of freedom. The model splits the difference between the measurements of the total cross section at $\sqrt{s} = 1800$ GeV (see Fig. 1). From Fig. 2, we note that the fit to ρ is anchored at $\sqrt{s} = 550$ GeV by the very accurate measurement[7] of UA4/2 and passes through the E710 point[8].

In Fig. 4 we show our *prediction* for the elastic cross section along with the data for both $\bar{p}p$ and pp. The agreement is excellent. We note that $\sigma_{elastic}$ is rising more

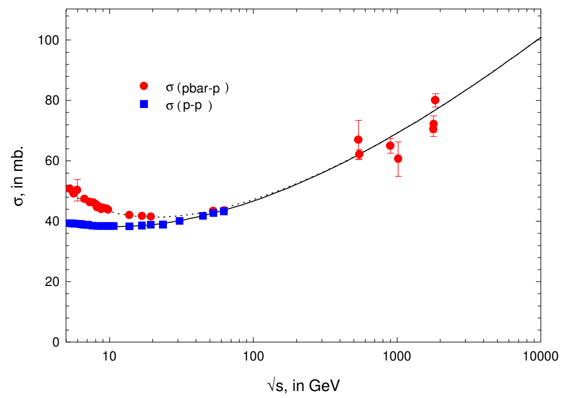

Figure 1: The total cross section for pp and $\bar{p}p$ scattering. The solid line and squares are for pp and the dotted line and circles are for $\bar{p}p$.

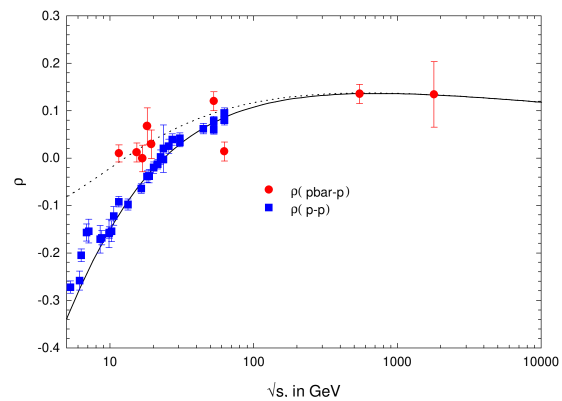

Figure 2: The ratio of the real to imaginary part of the forward scattering amplitude for pp and $\bar{p}p$ scattering. The solid line and squares are for pp and the dotted line and circles are for $\bar{p}p$.

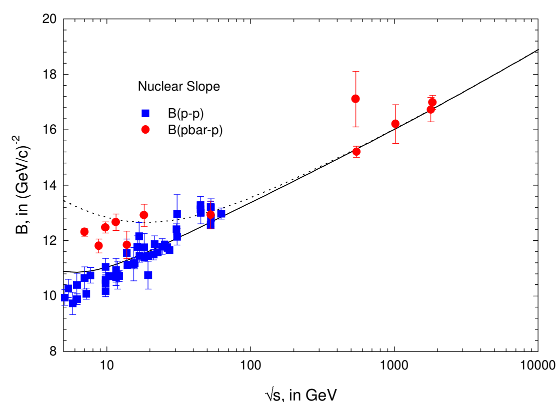

Figure 3: The nuclear slope parameter for elastic pp and $p\bar{p}$ scattering. The solid line and squares are for pp and the dotted line and circles are for $\bar{p}p$.

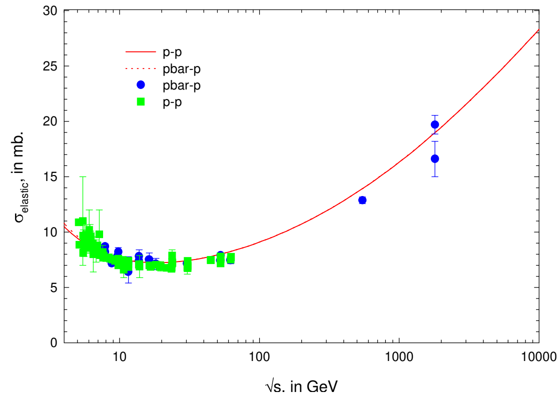

Figure 4: Elastic scattering cross sections for pp and $p\bar{p}$ scattering. The solid line and squares are for pp and the dotted line and circles are for $\bar{p}p$.

sharply with energy than the total cross section σ_{tot}. Comparing Fig. 1 with Fig. 4, we see that the ratio of the elastic to total cross section is rising with energy. The ratio is, of course, bounded by the value for the black disk[2,9], *i.e.,* 0.5, as the energy goes to infinity.

Having fixed all parameters specifying our eikonal, we can now predict $d\sigma/dt$, for various values of $\sqrt{s}$. The differential cross section at the Tevatron ($\sqrt{s} = 1800$ GeV) is shown in Fig. 5 along with E710[10] data. The agreement over 4 decades is

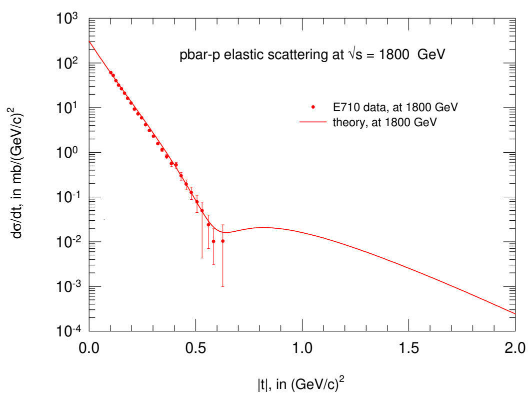

Figure 5: The elastic differential scattering cross section for the reaction $\bar{p}p \to \bar{p}p$ at $\sqrt{s} = 1800$ GeV. The data points are from E710.

striking. The differential cross section for $\sqrt{s} = 14$ TeV, the energy of the LHC, is plotted in Fig. 6. In particular, at small $|t|$, we predict that the curvature parameter C (see reference [1] for details) is negative. For energies much lower than 1800 GeV, the observed curvature has been measured as positive. For 1800 GeV, we see from Fig. 5 that the curvature parameter C is compatible with being zero. Block and Cahn[2,9] have pointed out that the curvature is predicted to go through zero near the

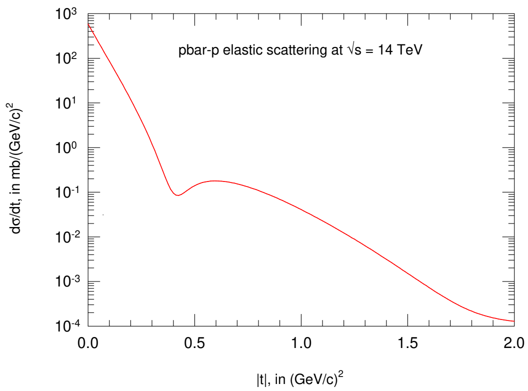

Figure 6: The elastic differential scattering cross section for the reaction $\bar{p}p \to \bar{p}p$ at LHC.

Tevatron energy and that it should become negative thereafter. Asymptotically the proton approaches a black disk. Its curvature is always negative[2,9)], $C = -R^4/192$, where R is the radius of the disk. Thus, the curvature has to pass through zero as the energy increases. 'Asymptopia' is the energy region (energies much larger than the Tevatron) where the scattering approaches that of a sharp disk.

3. γp and $\gamma\gamma$ Interactions

3.1. γp Reactions

We assume that the photon behaves like a two quark system when it interacts strongly[1)]. The γp scattering amplitudes are then obtained by performing the substitutions $\sigma_{ij} \to \frac{2}{3}\sigma_{ij}$ and $\mu_i \to \sqrt{\frac{3}{2}}\mu_i$ in the even eikonal for nucleon–nucleon scattering, so that

$$\chi^{\gamma p}(s,b) = i\left[\tfrac{2}{3}\sigma_{qq}(s)W\left(b;\sqrt{\tfrac{3}{2}}\mu_{qq}\right) + \tfrac{2}{3}\sigma_{qg}(s)W\left(b;\sqrt{\tfrac{3}{2}\mu_{qq}\mu_{gg}}\right) + \tfrac{2}{3}\sigma_{gg}(s)W\left(b;\sqrt{\tfrac{3}{2}}\mu_{gg}\right)\right]. \quad (10)$$

Using vector dominance, the photon-proton total cross section is then written as

$$\sigma_{tot}^{\gamma p}(s) = 2P_{had}\int \left\{1 - e^{-\chi_I^{\gamma p}(b,s)}\cos[\chi_R^{\gamma p}(b,s)]\right\} d^2\vec{b}, \quad (11)$$

where P_{had} is the probability that a photon interacts as a hadron. We use the value $P_{had} = 1/240$. This value is found by normalizing the total γp cross section to the low energy data, and is very close to that derived from vector dominance, $1/249$. Using $f_\rho^2/4\pi = 2.2$, $f_\omega^2/4\pi = 23.6$ and $f_\phi^2/4\pi = 18.4$, we find $\Sigma_V(4\pi\alpha/f_V^2) = 1/249$, where $V = \rho, \omega, \phi$ (see Table XXXV, pag. 393 of Ref. [11)]). With all eikonal parameters fixed by the nucleon-nucleon data, we can now calculate $\sigma_{tot}^{\gamma p}(s)$. The result is shown in

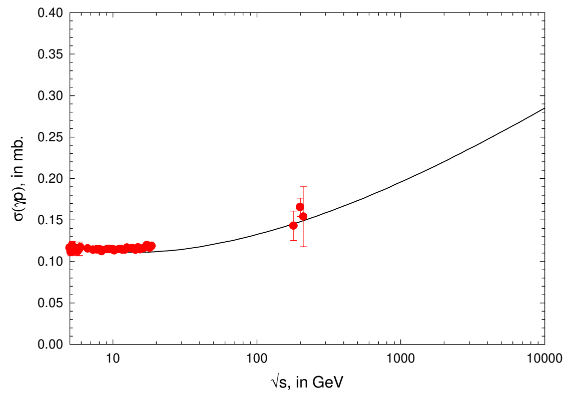

Figure 7: The total cross section for γp scattering.

Fig. 7. It reproduces the rising cross section for γp, using the parameters fixed by nucleon-nucleon scattering. The accuracy of our predictions are $\sim 1.5\%$, from the statistical uncertainty in our eikonal parameters.

We next consider the 'elastic' scatterings

$$\begin{aligned} \gamma + p &\rightarrow \rho_{virtual} + p \rightarrow \rho + p \ , \\ \gamma + p &\rightarrow \omega_{virtual} + p \rightarrow \omega + p \ , \\ \gamma + p &\rightarrow \phi_{virtual} + p \rightarrow \phi + p \ . \end{aligned} \qquad (12)$$

Here the photon virtually transforms into a vector meson which elastically scatters off of the proton. The strengths of these reactions is $\mathcal{O}(\alpha)$ times a strong interaction cross section. The true elastic cross section is given by Compton scattering on the proton, $\gamma + p \rightarrow \gamma + p$, which we can visualize as

$$\begin{aligned} \gamma + p &\rightarrow \rho_{virtual} + p \rightarrow \rho + p \rightarrow \gamma + p \ , \\ \gamma + p &\rightarrow \omega_{virtual} + p \rightarrow \omega + p \rightarrow \gamma + p \ , \\ \gamma + p &\rightarrow \phi_{virtual} + p \rightarrow \phi + p \rightarrow \gamma + p \ . \end{aligned} \qquad (13)$$

It is clearly $\mathcal{O}(\alpha^2)$ times a strong interaction cross section, and hence is much smaller than 'elastic' scattering of eq. (12). Thus, we justify the use of eq. (11) to calculate the total cross section, since only reactions with a photon in the final state are neglected.

We evaluate ρ and the slope B for the 'elastic' scattering expressed in eq. (12) using eq. (4) and (5). It can be seen from those equations that our predictions are free of P_{had} factors and are independent of normalization, it being the same for either ρp, ωp or ϕp final states.

The dependence of ρ with the energy is shown in Fig. 8. Damashek and Gilman[12)] have calculated the ρ value for Compton scattering on the proton using dispersion relations, *i.e.,* the true elastic scattering reaction for photon-proton scattering. We compare this calculation, the dotted line in Fig. 8, with our prediction of ρ (the solid

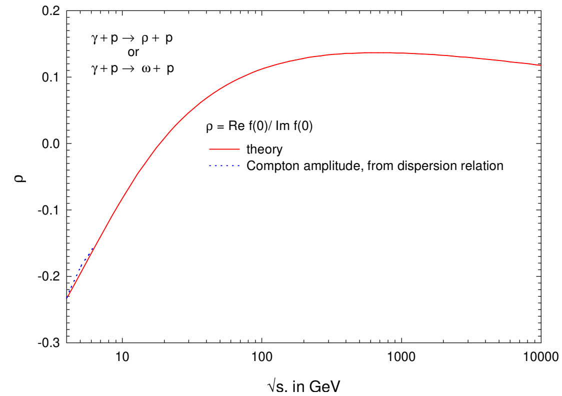

Figure 8: Ratio of the real to imaginary part of the forward scattering amplitude for the 'elastic' reactions $\gamma + p \rightarrow V_i + p$, where V_i is ρ^0, ω^0 or ϕ^0. The dotted curve is for Compton scattering from dispersion relations [12]. It has been slightly displaced from the solid curve for clarity in viewing.

line). The agreement is so close that we had to move the two curves apart so that they may be viewed more clearly.

In Fig. 9 we show our results for the slope B as a function of the energy. The

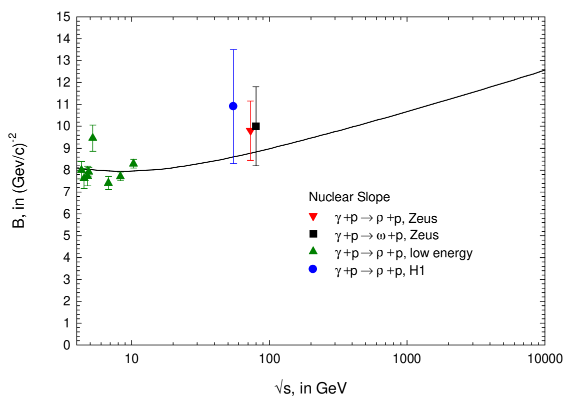

Figure 9: Nuclear slope parameter for the 'elastic' reaction $\gamma + p \rightarrow V_i + p$, where V_i is ρ^0, ω^0 or ϕ. For the reaction $\gamma + p \rightarrow \rho^0 + p$, the inverted triangles are the Zeus data, the circles are the H1 data, and the triangles are the low energy data. For the reaction $\gamma + p \rightarrow \omega^0 + p$, the squares are the Zeus data.

available experimental data for 'elastic' ρp and ωp final states are also plotted. Again, the agreement of theory and experiment is very good.

We note that the results for ρ and B are very critical to our analysis. We have assumed that, in some manner, the gluons are related to the quarks. For a two quark system, such as the photon, the factors of $2/3$ multiplying a cross section and $\sqrt{3/2}$ multiplying μ are the same for gluon-gluon as for quark-quark. If we relax this assumption and only use these factors in the quark, we get a sharp disagreement with our predicted ρ value, being considerably larger than the Compton value. The problem is further exacerbated in the predictions for B, with slopes from 11 GeV^{-2} (at 5 GeV) to 16 GeV^{-2} (at 80 GeV), which are much larger than the experimental values. This clearly has implications for constituent dynamics, which we will discuss further on.

To calculate the elastic cross sections $\sigma^{Vp}_{elastic}$ and differential cross sections $d\sigma^{Vp}/dt$ as a function of energy, we use

$$\sigma^{Vp}_{elastic}(s) = P^{Vp}_{had} \int \left|1 - e^{i\chi^{\gamma p}(b,s)}\right|^2 \, d^2\vec{b}, \tag{14}$$

where P^{Vp}_{had} is the appropriate probability for a photon to turn into V, with $V = \rho,\ \omega$ or ϕ. The differential scattering cross section is given by

$$\frac{d\sigma^{Vp}}{dt}(s,t) = \frac{P^{Vp}_{had}}{4\pi} \left|\int J_0(qb)(1 - e^{i\chi^{\gamma p}(b,s)})\, d^2\vec{b}\right|^2, \tag{15}$$

where $t = -q^2$.

The differential cross section, $d\sigma/dt$, for the 'elastic' reactions $\gamma + p \rightarrow \rho^0 + p$, $\gamma + p \rightarrow \omega^0 + p$ and $\gamma + p \rightarrow \phi^0 + p$ are plotted in Figs. 10, 11, and 12, respectively. The agreement, in absolute normalization and shape, of our results for all three

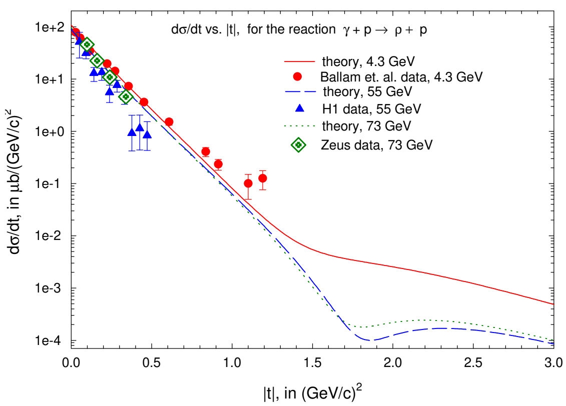

Figure 10: The differential cross section for the 'elastic' reaction $\gamma + p \rightarrow \rho^0 + p$. The solid curve and the circles (Ballam *et al.* data) are at $\sqrt{s}$= 4.3 GeV, the dashed curve and triangles (H1 data) are at $\sqrt{s}$= 55 GeV, and the dotted curve and diamonds are at $\sqrt{s}$= 73 GeV (Zeus data).

light vector mesons with the experimental data for all available energies reinforces our confidence in the model.

3.2. $\gamma\gamma$ Total Cross Section

We now consider $\gamma\gamma$ interactions. As it was done for γp interactions, we will start from the eikonal $\chi^{\gamma p}(s,b)$ and multiply every cross section by 2/3 and multiply each

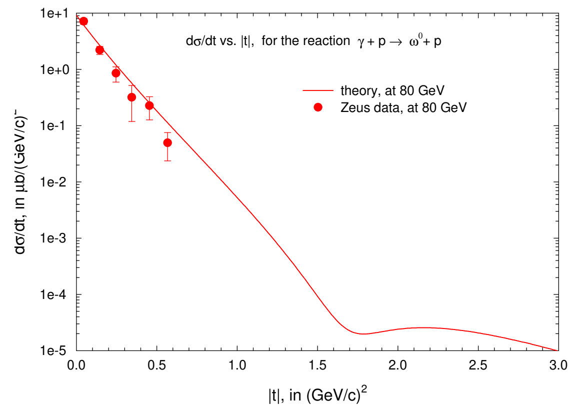

Figure 11: The differential cross section for the 'elastic' reaction $\gamma + p \rightarrow \omega^0 + p$ at $\sqrt{s}$=80 GeV. The circles are the Zeus data.

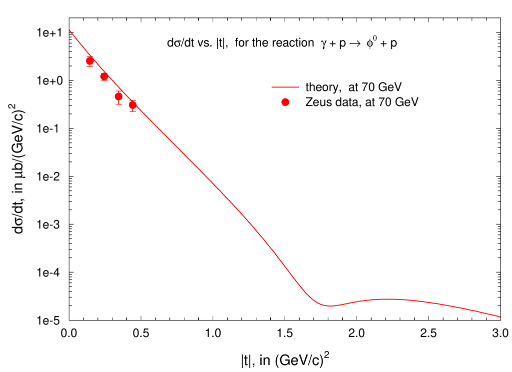

Figure 12: The differential cross section for the 'elastic' reaction $\gamma + p \rightarrow \phi^0 + p$ at $\sqrt{s}$=70 GeV. The circles are the Zeus data.

μ by $\sqrt{3/2}$. Therefore,

$$\chi^{\gamma\gamma}(s,b) = i\left[\tfrac{4}{9}\sigma_{qq}(s)W\left(b;\tfrac{3}{2}\mu_{qq}\right) + \tfrac{4}{9}\sigma_{qg}(s)W\left(b;\tfrac{3}{2}\sqrt{\mu_{qq}\mu_{gg}}\right) + \tfrac{4}{9}\sigma_{gg}(s)W\left(b;\tfrac{3}{2}\mu_{gg}\right)\right]. \tag{16}$$

Using vector dominance we obtain,

$$\sigma_{tot}^{\gamma\gamma}(s) = 2P_{had}^2 \int \left\{1 - e^{-\chi_I^{\gamma\gamma}(b,s)}\cos[\chi_R^{\gamma p}(b,s)]\right\} d^2\vec{b}, \tag{17}$$

where $P_{had} = 1/240$ is the probability that a photon will interact as a hadron. In Fig. 13 we plot our results for $\sigma_{tot}^{\gamma\gamma}(s)$ as a function of the energy, and compare it to

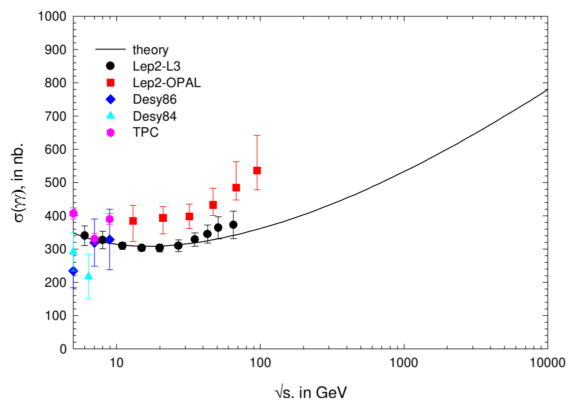

Figure 13: The total cross section for $\gamma\gamma$ scattering. The data sources are indicated in the legend.

the various sets of experimental data. We note that it gives good agreement with the data set for Lep2-L3.

We have used the factorization theorem, $\sigma_{\rm nn}/\sigma_{\gamma p} = \sigma_{\gamma p}/\sigma_{\gamma\gamma}$, in the various eikonals for nn, γp and $\gamma\gamma$, in our model. Interestingly, Block and Kaidalov[13)] have shown that this theorem holds exactly, *even after eikonalization*, when an additive quark model and vector dominance is assumed, with the proportionality constant $2/(3P_{\rm had}^{\gamma})$. This result is numerically born out in Figures 1, 7 and 13.

4. A Global Fit Simultaneously using Cosmic Ray and Accelerator Data

In this section, we will discuss the results of a global fit, simultaneously using cosmic ray and accelerator data, work done by Block, Halzen and Stanev[14)].

4.1. Cosmic Ray Analysis

Cosmic ray experiments measure the penetration in the atmosphere of particles with energies in excess of those accelerated by existing machines—interestingly, their energy range covers the energy of the Large Hadron Collider (LHC) and extends beyond it. However, extracting proton–proton cross sections from cosmic ray observations is far from straightforward[15]. By a variety of experimental techniques, cosmic ray experiments map the atmospheric depth at which cosmic ray initiated showers develop. The measured quantity is the shower attenuation length (Λ_m), which is not only sensitive to the interaction length of the protons in the atmosphere ($\lambda_{p-\mathrm{air}}$), with

$$\Lambda_m = k\lambda_{p-\mathrm{air}} = k\frac{14.5m_p}{\sigma_{p-\mathrm{air}}^{\mathrm{inel}}}\,, \tag{18}$$

but also depends on the rate at which the energy of the primary proton is dissipated into electromagnetic shower energy observed in the experiment. The latter effect is parameterized in Eq. (18) by the parameter k; m_p is the proton mass and $\sigma_{p-\mathrm{air}}^{\mathrm{inel}}$ the inelastic proton-air cross section. The value of k depends on the inclusive particle production cross section in nucleon and meson interactions on the light nuclear target of the atmosphere and its energy dependence.

The extraction of the pp cross section from the cosmic ray data is a two step process. First, one calculates the p-air total cross section from the inelastic cross section inferred in Eq. (18), where

$$\sigma_{p-\mathrm{air}}^{\mathrm{inel}} = \sigma_{p-\mathrm{air}} - \sigma_{p-\mathrm{air}}^{\mathrm{el}} - \sigma_{p-\mathrm{air}}^{q-\mathrm{el}}\,. \tag{19}$$

Next, the Glauber method[16] is used to transform the value of $\sigma_{p-\mathrm{air}}^{\mathrm{inel}}$ into a proton–proton total cross section σ_{pp}; all the necessary steps are calculable in the theory. In Eq. (19) the cross section for particle production is supplemented with $\sigma_{p-\mathrm{air}}^{\mathrm{el}}$ and $\sigma_{p-\mathrm{air}}^{q-\mathrm{el}}$, the elastic and quasi-elastic cross section, respectively, as calculated by the Glauber theory, to obtain the total cross section $\sigma_{p-\mathrm{air}}$. The subsequent relation between $\sigma_{p-\mathrm{air}}^{\mathrm{inel}}$ and σ_{pp} involves the slope of the forward scattering amplitude for elastic pp scattering, $\frac{d\sigma_{pp}^{\mathrm{el}}}{dt}$,

$$B = \left[\frac{d}{dt}\left(\ln\frac{d\sigma_{pp}^{\mathrm{el}}}{dt}\right)\right]_{t=0}\,, \tag{20}$$

and is shown in Fig. 14, which plots B against σ_{pp}, for 5 curves of different values of $\sigma_{p-\mathrm{air}}^{\mathrm{inel}}$. This summarizes the reduction procedure from the measured quantity Λ_m (of Eq. 18) to σ_{pp}[15]. Also plotted in Fig. 14 is a curve of B *vs.* σ_{pp} which will be discussed later.

A significant drawback of the method is that one needs a model of proton–air interactions to complete the loop between the measured attenuation length Λ_m and the cross section $\sigma_{p-\mathrm{air}}^{\mathrm{inel}}$, *i.e.,* the value of k in Eq. (18). Our method of analysis minimizes the impact of theory, by not requiring models.

4.2. Global Analysis

We have constructed a QCD-inspired parameterization of the forward proton–proton and proton–antiproton scattering amplitudes[17] which is analytic, unitary and

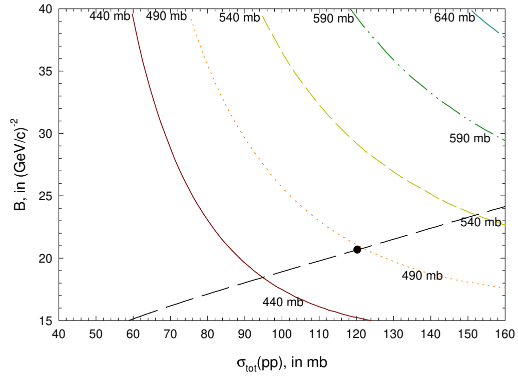

Figure 14: B dependence on the pp total cross section σ_{pp}. The five curves are lines of constant $\sigma^{\rm inel}_{p-{\rm air}}$, of 440, 490, 540, 590 and 640 mb—the central value is the *published* Fly's Eye value, and the others are $\pm 1\sigma$ and $\pm 2\sigma$. The dashed curve is a plot of our QCD-inspired fit of B against σ_{pp}. The dot is our fitted value for $\sqrt{s} = 30$ TeV, the Fly's Eye energy.

essentially model-free. It fits all accelerator data of $\sigma_{\rm tot}$, B and ρ, the ratio of the real-to-imaginary part of the forward scattering amplitude; see Fig. 15. In addition, the

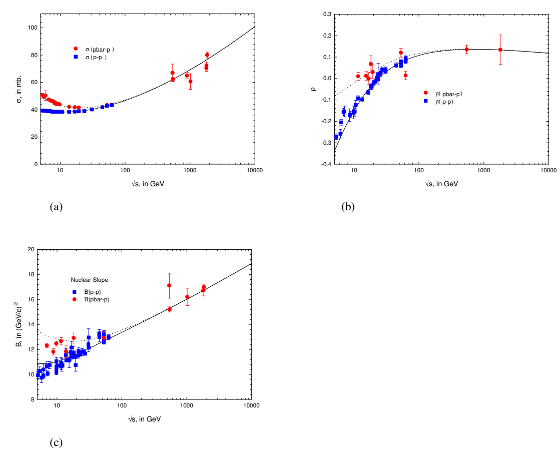

Figure 15: The simultaneous QCD-inspired fit of total cross section σ_{pp}, ρ and B *vs.* $\sqrt{s}$, in GeV, for pp (squares) and $\bar{\rm p}$p (circles) accelerator data: (a) σ_{pp}, in mb, (b) ρ, (c) Nuclear slope B, in GeV^{-2}

high energy cosmic ray data are also simultaneously used, *i.e.*, k from Eq.(18) is also a fitted quantity—we refer to this fit as a *global* fit[14)]. We emphasize that in the global fit, all 4 quantities, $\sigma_{\rm tot}$, B, ρ and k, are *simultaneously* fitted. Using vector meson dominance and the additive quark models, our QCD fit accommodates a wealth of data on photon-proton and photon-photon interactions without the introduction of new parameters, as shown earlier. Because the model is both unitary and analytic, it

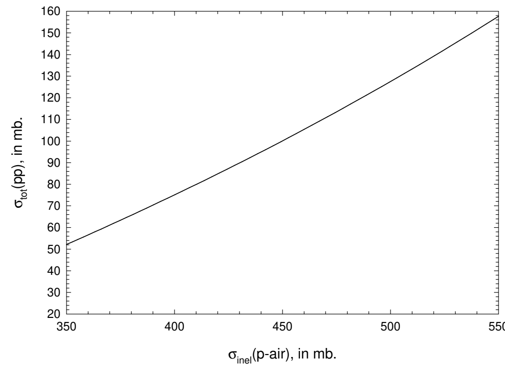

Figure 16: A plot of the predicted total pp cross section σ_{pp}, in mb *vs.* the measured p-air cross section, $\sigma_{p-\mathrm{air}}^{\mathrm{inel}}$, in mb.

has high energy predictions that are essentially theory–independent. In particular, it also *simultaneously* fits σ_{pp} and B, forcing a relationship between the two. Specifically, the B *vs.* σ_{pp} prediction of the model is shown as the dashed curve in Fig. 14. The dot corresponds to our prediction of σ_{pp} and B at $\sqrt{s} = 30$ TeV. It is seen to be slightly below the curve for 490 mb, the lower limit of the Fly's Eye measurement, which was made at $\sqrt{s} \approx 30$ TeV. The percentage error in the prediction of σ_{pp} at $\sqrt{s} = 30$ TeV is $\approx 1.2\%$, due to the statistical error in the fitting parameters (see references [17],[1]).

In Fig. 16, we have plotted the values of σ_{pp} *vs.* $\sigma_{p-\mathrm{air}}^{\mathrm{inel}}$ that are deduced from the intersections of the B-σ_{pp} curve with the $\sigma_{p-\mathrm{air}}^{\mathrm{inel}}$ curves of Fig. 14. Figure 16 allows the conversion of the measured $\sigma_{p-\mathrm{air}}^{\mathrm{inel}}$ to σ_{pp} . The percentage error in $\sigma_{p-\mathrm{air}}^{\mathrm{inel}}$ is ≈ 0.8 % near $\sigma_{p-\mathrm{air}}^{\mathrm{inel}} = 450$mb, due to the error in σ_{pp} from the model parameter uncertainties.

Our prediction for the total cross section σ_{pp} as a function of energy is confronted with all of the accelerator and cosmic ray measurements[18,19,20] in Fig. 17. For inclusion in Fig. 17, we have calculated the cosmic ray values of σ_{pp} from the *published* experimental values of $\sigma_{p-\mathrm{air}}^{\mathrm{inel}}$, using the results of Fig. 16. We note the systematic underestimate of the cosmic ray points, roughly about the level of one standard deviation.

It is at this point important to recall Eq. (18) and consider the fact that the extraction of $\sigma_{p-\mathrm{air}}^{\mathrm{inel}}$ from the measurement of Λ_m requires a determination of the parameter k. The measured depth $X_{\max}$ at which a shower reaches maximum development in the atmosphere, which is the basis of the cross section measurement in Ref. [18], is a combined measure of the depth of the first interaction, which is determined by the inelastic cross section, and of the subsequent shower development, which has to be corrected for. The position of $X_{\max}$ also directly affects the rate of shower attenuation with atmospheric depth which is the alternative procedure for extracting $\sigma_{p-\mathrm{air}}^{\mathrm{inel}}$.

The model dependent rate of shower development and its fluctuations are the

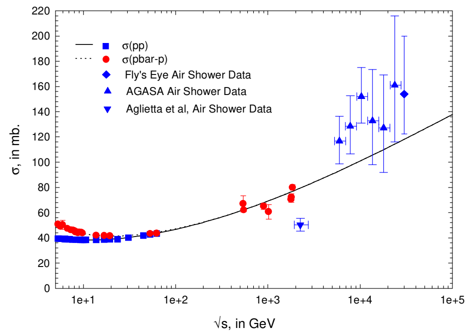

Figure 17: A plot of the QCD-inspired fit of the total nucleon-nucleon cross section σ_{pp}, in mb *vs.* $\sqrt{s}$, in GeV. The cosmic ray data that are shown have been converted from $\sigma_{p-\rm air}^{\rm inel}$ to σ_{pp} using the results of Fig. 16 and the *published* values of $\sigma_{p-\rm air}^{\rm inel}$.

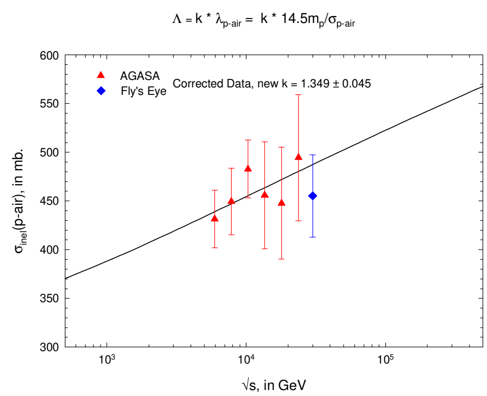

Figure 18: The AGASA and Fly's Eye data for $\sigma_{p-\rm air}^{\rm inel}$, in mb, as a function of the energy, $\sqrt{s}$, in GeV, as found in our global fit, using the common value of $k = 1.349$

origin of the deviation of k from unity in Eq. (18). Its values range from 1.5 for a model where the inclusive cross section exhibits Feynman scaling, to 1.1 for models with large scaling violations[15)]. The comparison between data and experiment in Fig. 17 is further confused by the fact that the AGASA[19)] and Fly's Eye[18)] experiments used different values of k in the analysis of their data, *i.e.,* AGASA used $k = 1.5$ and Fly's Eye used $k = 1.6$.

We therefore decided to let k be a free parameter and make a global fit to the accelerator and cosmic ray data, as mentioned above. This neglects the possibility that k may show a weak energy dependence over the range measured. We find that $k = 1.349 \pm 0.045$, where the error in k is the statistical error of the fit. By combining the results of Fig. 15 (a) and Fig. 16, we can plot our prediction of $\sigma_{p-\rm air}^{\rm inel}$ *vs.* $\sqrt{s}$. In Fig. 18 we have rescaled the published high energy data for $\sigma_{p-\rm air}^{\rm inel}$ (using the common

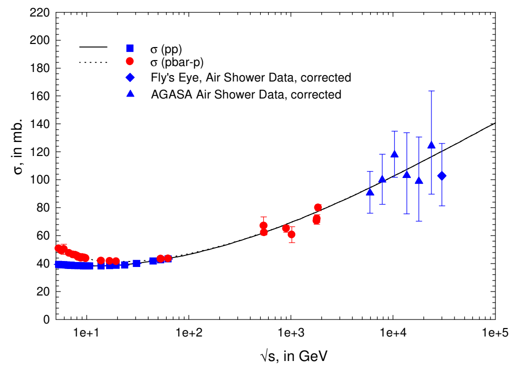

Figure 19: A plot of the QCD-inspired fit of the total nucleon-nucleon cross section σ_{pp}, in mb *vs.* $\sqrt{s}$, in Gev. The cosmic ray data that are shown have been converted from $\sigma^{\rm inel}_{p-{\rm air}}$ to σ_{pp} using the results of Fig. 16 and the common value of $k = 1.349$, found from our global fit.

value of $k = 1.349$), and plotted the rescaled data against our prediction of $\sigma^{\rm inel}_{p-{\rm air}}$ *vs.* $\sqrt{s}$. Clearly, we have an excellent fit, with good agreement between AGASA and Fly's Eye. The plot of σ_{pp} *vs*$\sqrt{s}$, including the *revised* cosmic ray data is shown in Fig. 19. Our result for k is interesting—it is close to the value of 1.2 obtained using the SIBYLL simulation[21)] for inclusive particle production. This represents a consistency check in the sense that our model for forward scattering amplitudes and SIBYLL share the same underlying physics. The increase of the total cross section with energy to a black disk of soft partons is the shadow of increased particle production which is modeled by the production of (mini)-jets in QCD. The difference between the k values of 1.20 and 1.349 could be understood because the experimental measurement integrates showers in a relatively wide energy range, which tends to increase the value of k.

4.3. Parameterization of $\sigma^{\rm inel}_{p-{\rm air}}$

A simple parameterization for the inelastic p-air cross section over the proton laboratory energy region 10^{14} to 10^{20} ev is given by

$$\sigma^{\rm inel}_{p-{\rm air}} = \sigma_0[1 + a_0 \ln(E_{\rm lab}/1000)], \qquad (21)$$

where $\sigma_0 = 297.20$ mb, $a_0 = 0.04879$ and $E_{\rm lab}$ is the laboratory energy of the proton, in GeV, and is shown in Fig. 20. This parameterization of our theory can be useful in the calculation of neutrino fluxes needed in neutrino telescope experiments.

4.4. Predictions for the LHC

We predict at the LHC energy (14 TeV), that $\sigma_{\rm total} = 107.4 \pm 1.5$ mb, $\sigma_{\rm elastic} = 30.9 \pm 0.5$ mb, $\rho = 0.112 \pm 0.002$, and $B = 19.41 \pm 0.15$ Gev^{-2}, where the quoted

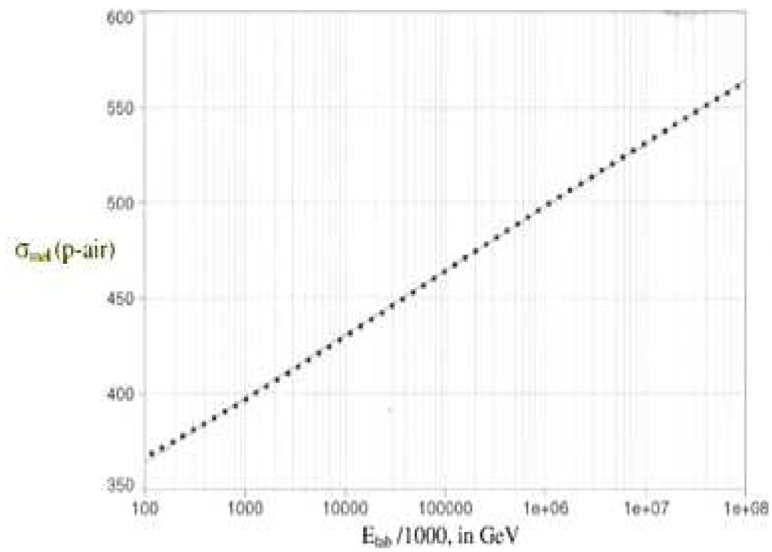

Figure 20: A convenient parameterization of $\sigma_{p-\mathrm{air}}^{\mathrm{inel}}$, the inelastic p-air cross section, in mb vs. E_{lab}, the laboratory energy of the proton, in GeV. The dots are numerical calculations using our theory, and the solid line is the parameterization given in the text.

errors are due to the statistical errors of the fitting parameters.

5. Conclusions

The overall agreement between the accelerator data and the cosmic ray data with our QCD-inspired fit, as shown in Fig. 19, is striking. Thus, the accelerator and cosmic ray data are readily reconcilable, if we use a (model independent) value of $k = 1.349 \pm 0.045$.

6. Acknowledgements

This work was supported in part by the Department of Energy under Grant no. DA-AC02-76-Er02289 Task D.

7. References

1) M. M. Block *et al.*, e-Print Archive: **hep-ph/9809403**, Phys. Rev. D**60**, 054024 (1999).
2) M. M. Block and R. N. Cahn, Rev. Mod. Phys. **57**, 563 (1985).
3) Eden, R. J., “High Energy Collisions of Elementary Particles”, Cambridge University Press, Cambridge (1967).

4) C. Avila *et al.*, Phys. Lett. B **445**, 419 (1999).
5) E710 Collaboration, N. Amos *et al.*, Phys. Rev. Lett. **63**, 2784 (1989).
6) CDF Collaboration, F. Abe *et al.*, Phys. Rev. D **50**, 5550 (1994).
7) UA4 Collaboration, C. Augier *et al.*, Phys. Lett. B **316**, 448 (1993).
8) E710 Collaboration, N. Amos *et al.*, Phys. Rev. Lett. **68**, 2433 (1992).
9) M. M. Block and R. N. Cahn, Phys. Lett. B **149**, (1984).
10) E710 Collaboration, N. Amos *et al.*, Phys. Rev. Lett. **61**, 525 (1988).
11) T. H. Bauer *et al.*, Rev. Mod. Phys. **50**, 261 (1978).
12) M. Damashek and F. J. Gilman, Phys. Rev. D **1**,1319 (1970).
13) M. M. Block and A. B. Kaidalov, "Consequences of the Factorization Hypothesis in $\bar{p}p$, pp, γp and $\gamma\gamma$ Collisions", e-Print Archive: **hep-ph/0012365**, Northwestern University preprint N.U.H.E.P No. 712, Nov. 2000.
14) M. M. Block *et al.*, Phys. Rev. D**62**, 077501, 2000. In an earlier communication, we had first fit the accelerator data alone. Using the parameters from this fit, we then made a *separate* fit of the cosmic ray data to the value of k; see M. M. Block *et al.*, Phys. Rev. Lett. **83**, 4926, 1999. In this work, we make a simultaneous fit of the accelerator *and* the cosmic ray data, a much more complicated and very lengthy numerical analysis, but a superior physical analysis.
15) R. Engel *et al.*, Phys. Rev. D**58**, 014019, 1998.
16) T. K. Gaisser *et al.*, Phys. Rev. D**36**, 1350, 1987.
17) M. M. Block *et al.*, Phys. Rev. D**45**, 839, 1992.
18) R. M. Baltrusaitis *et al.*, Phys. Rev. Lett. **52**, 1380, 1984.
19) M. Honda *et al.*, Phys. Rev. Lett. **70**, 525, 1993.
20) M. Aglietta *et al*, Proc 25th ICRC (Durban) **6**, 37, 1997.
21) R. S. Fletcher *et al.*, Phys. Rev. D**50**, 5710, 1994.